Organic Communications
www.acgpubs.org
Open Access
This article is licensed under CC-BY-NC-ND 4.0
ORIGINAL ARTICLE

Ionic lipid–surfactant complex based on phosphatidylcholine and sodium dodecyl sulfate for enhanced curcumin encapsulation and sustained delivery

Aysegul Yargic[1], Fatemeh Bahadori[2], Muge Sennaroglu Bostan[1] and Mehmet S. Eroglu[3*]

[1]Marmara University, Engineering Faculty, Department of Chemical Engineering, Aydınevler Maltepe, Istanbul 34854, Türkiye
[2]Istanbul University-Cerrahpasa, Faculty of Pharmacy, Department of Analytical Chemistry, Avcilar Campus, Istanbul 34500, Türkiye
[3]Department of Metallurgical and Materials Engineering, Technology Faculty, Marmara University, Aydınevler, Maltepe, Istanbul 34854, Türkiye

Cite This: *Org. Commun.* 2026, 19(4), e26083994

Read Online

Abstract: Developing stable, efficient nanocarriers for hydrophobic anticancer agents remains a major challenge in pharmaceutical nanotechnology. In this study, we engineered a novel ion-pair amphiphile through electrostatic complexation between zwitterionic phosphatidylcholine and the anionic surfactant sodium dodecyl sulfate (SDS), forming a phosphatidylcholine–SDS (P-SDS) ionic complex with enhanced hydrophobicity and self-assembly capability. The resulting hybrid amphiphile was further stabilized with Tween-80 and formulated into nanoscale micellar structures to encapsulate curcumin. ^{1}H-NMR and FT-IR spectroscopy confirmed the formation of the P-SDS ionic complex, while DSC analysis showed the disappearance of crystalline curcumin, indicating successful amorphous dispersion within the micellar core. Fluorescence spectroscopy revealed a low critical micelle concentration (CMC) of 3.1×10^{-4} M, suggesting favorable thermodynamic stability of the self-assembled system. Dynamic light scattering measurements showed an average particle size of approximately 239 nM with a strongly negative zeta potential ranging from −37 to −44 mV, indicating good colloidal stability. The optimized formulation achieved 19% drug loading with an encapsulation efficiency of 39.8%. In vitro release studies showed a biphasic release profile: an initial moderate burst followed by sustained curcumin release over 72 h. Morphological analyses using ESEM and TEM confirmed the formation of spherical nanoscale assemblies with relatively uniform morphology. The developed P-SDS nanoassembly is a simple, scalable, and biocompatible platform for delivering hydrophobic therapeutic agents. The ion-pair engineering strategy proposed in this work provides a versatile approach to tuning amphiphilicity, self-assembly behavior, and drug-loading capacity in lipid-based nanocarriers, with potential applicability for passive tumor targeting through the enhanced permeability and retention (EPR) effect.

Keywords: Curcumin, lecithin, phosphatidylcholine, nano-formulation, ionic complex

1 Introduction

Nanoparticle-based drug delivery systems have transformed modern chemotherapy by improving pharmacokinetics, enhancing bioavailability, and reducing systemic toxicity. Despite extensive progress, clinical translation of many nanocarriers remains limited because of challenges such as insufficient drug loading, poor structural stability, and complex fabrication processes.[1–3] Therefore, designing simple, biocompatible, and highly efficient delivery platforms remains a critical research priority in pharmaceutical nanotechnology.

A major limitation in anticancer therapy is the inherently poor aqueous solubility of many chemotherapeutic agents, which leads to low bioavailability and rapid systemic clearance. Hydrophobic drugs typically exist in crystalline form, which further restricts their dissolution in physiological media. To address this issue, amphiphilic nanostructures such as micelles and lipid-based carriers have been widely investigated because they can encapsulate hydrophobic molecules within their hydrophobic cores, enhancing solubility and enabling sustained release profiles.

*Corresponding Author: Mehmet S. Eroglu. Email: mehmet.eroglu@marmara.edu.tr
Received: August 05, 2026
Revised: September 30, 2026
Accepted: September 30, 2026
Published: November 02, 2026

Copyright © 2026. Published by ACG Publications.

In addition, these nanosystems may improve tumor accumulation through the enhanced permeability and retention (EPR) effect, a widely exploited mechanism for passive targeting of solid tumors.[4–6]

Phosphatidylcholine, a naturally occurring zwitterionic phospholipid and a major component of biological membranes, has been widely used in drug delivery applications because of its excellent biocompatibility, biodegradability, and regulatory acceptance.[5–8] Its amphiphilic structure enables spontaneous assembly into vesicular and micellar systems, making it a suitable candidate for drug carrier design.[9–12] However, its structural limitations often restrict drug-loading capacity and physicochemical stability in complex biological environments.

To overcome these limitations, researchers have explored surfactant-assisted modification strategies. Sodium dodecyl sulfate (SDS), an anionic surfactant widely used in pharmaceutical formulations, enhances solubility, stabilizes colloidal systems, and promotes micelle formation. Moreover, SDS can modulate membrane permeability, which may improve intracellular delivery of encapsulated agents. Despite these advantages, combining phospholipids and ionic surfactants to construct stable drug carriers remains underexplored.[13–15]

Curcumin (Cur), a hydrophobic polyphenolic compound derived from *Curcuma longa*, has attracted considerable attention due to its broad spectrum of biological activities, including anticancer, anti-inflammatory, antioxidant, and antimicrobial effects. However, poor aqueous solubility, low systemic bioavailability, and rapid metabolic degradation under physiological conditions severely restrict its clinical application.[16–18] Previous studies have shown that Cur decomposes rapidly in physiological buffers, further limiting its therapeutic efficacy. Consequently, developing efficient delivery systems that protect Cur from degradation while enhancing its solubility and stability is important.[19–24] Cur is a compound classified as "Generally Recognized as Safe" by the Food and Drug Administration (FDA).[22,23]

Therefore, an efficient delivery system is needed to protect Cur from degradation while enhancing its solubility and bioavailability.[25,26] Hence, Oetari et al. (1996) and Pan, Huang et al. (1999) found that over 90% of Cur decomposes in phosphate buffer solution (PBS, pH 7.4).[25,26] Delivering Cur to the specific site of cancer cells with a protective carrier system is necessary to increase bioavailability and prevent physiological degradation.

In the present study, we report the development of a novel phosphatidylcholine–sodium dodecyl sulfate ionic complex (P-SDS) formed via ion-pair interaction. This system generates a structurally stable amphiphilic assembly with enhanced hydrophobicity and improved drug-loading capacity. The P-SDS complex was further formulated into nano-micelles using Tween-80 as a stabilizing agent and employed for Cur encapsulation. It is noteworthy that, all chemicals used in the formulation are FDA-approved.[27] We systematically investigated the physicochemical properties, structural characteristics, and drug-release behavior of the resulting nanoformulation to evaluate its potential as a biocompatible and efficient anticancer drug-delivery platform.

2 Experimental

2.1 Materials

L-α-Phosphatidylcholine derived from soybean lecithin (CAS No: 8002-43-5, GPR grade) was purchased from VMR Prolabo (Leuven, Belgium). Sodium dodecyl sulfate (SDS, ≥98% purity, CAS No: 151-21-3) was obtained from Fisher BioReagents (China). Cur (≥95% purity, CAS No: 458-37-7), Tween 80 (polyoxyethylene sorbitan monooleate, CAS No: 9005-65-6), and pyrene (CAS No: 129-00-0) were purchased from Sigma-Aldrich (USA). Dichloromethane (DCM, analytical grade, CAS No: 75-09-2) and all other solvents were obtained from Merck (Germany). Phosphate-buffered saline (PBS, pH 7.4) was prepared from commercial tablets containing NaCl (0.137 M), KCl (0.0027 M), and phosphate buffer (0.01 M). All reagents were used without further purification.

2.2 Instrumentation

Nuclear magnetic resonance (^{1}H NMR) characterization of SDS, Phosphatidylcholine, and the P-SDS complex was performed using a Varian 600 MHz NMR instrument at room temperature. The ^{1}H NMR spectra of phosphatidylcholine and the P-SDS complex were recorded in $CDCl_3$, while that of SDS was recorded in D_2O. Proton chemical shifts were recorded in ppm downfield from tetramethylsilane (TMS). We recorded phosphatidylcholine and P-SDS complex spectra using a Thermo Nicolet 6700 Fourier transform infrared (FT-IR) spectrophotometer equipped with Smart Orbit high-performance diamond attenuated total reflectance (ATR) accessories. To assess the compatibility of SDS, phosphatidylcholine, and Cur in bulk nano-micelles, differential scanning calorimetry (DSC) was used. Measurements (4–6 mg of the samples) were performed using a Perkin Elmer Jade DSC instrument at a heating rate of 10°C/min under a dynamic argon atmosphere with a 200 mL/min flow rate. The data were processed using Pyris software. The compositional analyses of the nano-structured P-SDS micelles and the P-SDS ionic complex in bulk form were performed using the thermal gravimetric analysis (TGA) technique. Measurements were conducted using a Seiko EXSTAR TG/DTA 7300 model thermal analyzer under a dynamic nitrogen atmosphere (200 mL/min flow rate) at 10°C/min heating rate. Approximately 5 mg of the samples were used in each measurement. Before each measurement, the samples were pre-heated to 110°C to remove water and solvent, and then TGA thermograms were recorded.

Cur release from nano-micelles formed by the SDS-phosphatidylcholine complexes was determined using an Agilent Technologies Cary-60 UV-VIS spectrophotometer. Spectra were recorded between 200–800 nM at 25°C. The Cur release was followed at predetermined time intervals. The measurements were performed at regular time intervals with 3.0 mL of samples. The Cur release profile of the nano-micelles was determined from the UV-Vis calibration curve. Scanning electron microscopy images of the Cur-loaded micelles were obtained using HITACHI 5000 VP-FEG-SEM&EDS, installed with Schottky Gun and DEBEN-TEM detector.

https://doi.org/10.25135/org.2608.3994
Org. Commun. 2026, 19(4):e26083994

Environmental SEM images (ESEM) of the nano-micelles were recorded in a wet environment using the QX-102 imaging capsule. Before recording the SEM images, the inner surface of the imaging capsule was coated with a positively charged poly-l-lysine to fix the negatively charged nano-micelles on the coated surface.15 µL of QX-102 Imaging Buffer was added before imaging to minimize potential damage to the NP surface by the electron beam, and 15 µL of QX-102 Imaging Buffer was added before imaging. ESEM images were recorded at 30 kV acceleration voltage with 50K and 90K magnifications. Transmission electron microscopy (TEM) was also used to image the nano-micelles. Before taking the TEM images, a drop of aqueous nano-micelle dispersion was applied on a carbon-coated Cu TEM grid (300 mesh) and waited 30 minutes to dry at room temperature. TEM images were recorded at 30 kV acceleration voltage with 18K and 50K magnification. Average particle size, particle size distribution, and zeta potential value of the Cur loaded nano-structured micelles (Cur-P-SDS) were determined using Zetasizer Nano-ZSP (Malvern Instruments, UK) model dynamic light scattering (DLS) instrument with a laser diode illuminated light scattering sensor at 25°C. Before measurements, samples were kept at room temperature for 24 hours. Five measurements were averaged for each sample, and particle size distribution was presented as intensity (percent). The fluorescence measurements determined critical micelle concentration (CMC) using an FS2 model fluorescence spectrophotometer (Scinco) with FloroMaster FS-2 software. Pyrene was used as a fluorescent probe. A Biosan ES-20F model orbital shaker-incubator was used for release studies. The samples were shaken at 37°C, 100 rpm in a thermostatically controlled incubator.

2.3 Preparation of Phosphatidylcholine–SDS Ionic Complex (P-SDS)

The phosphatidylcholine–SDS (P-SDS) ionic complex was prepared via ion-pair self-assembly. Briefly, phosphatidylcholine (0.2 M) and SDS (0.2 M) were mixed in water and heated to 80°C until a clear dispersion was obtained. After cooling to room temperature, the mixture was vortexed for 30 min to promote electrostatic interactions between the oppositely charged groups. The resulting mixture was lyophilized at −60°C under vacuum to stabilize the ionic complex. The dried product was extracted using dichloromethane (DCM) to remove unbound components and further dried in a vacuum oven at 30°C for 24 h. The obtained yellowish creamy ionic P-SDS complex was characterized using FT-IR and ^{1}H-NMR spectroscopy and stored at 4°C until further use. The systematic formation of the P-SDS ionic complex is given in Figure 1.

2.4 Determination of Critical Micelle Concentration (CMC)

The critical micelle concentration (CMC) of the P-SDS complex was determined using pyrene as a hydrophobic fluorescent probe. Pyrene was dissolved in acetone (6×10^{-7} M), and equal volumes were distributed into test tubes. The solvent was evaporated to form a thin pyrene film at the bottom of each tube. P-SDS containing 0.2 M phosphatidylcholine and 0.2 M SDS was prepared as mentioned above. After preparation of P-SDS, 30 serially diluted solutions were subsequently obtained by two-fold dilution, with the concentration reduced by half at each successive dilution step in PBS (pH 7.4). These solutions were added on the pre-dried Pyrene tubes followed by vortexing (2 min) and sonication (5 min). After equilibration for 2 h at room temperature, fluorescence emission spectra were recorded at an excitation wavelength of 343 nM. Background fluorescence was corrected by subtracting the spectrum of the corresponding pyrene-free P-SDS solution measured under identical instrumental conditions. The CMC was determined from the breakpoint in the plot of the pyrene fluorescence intensity ratio (I_1/I_3, 386 nM/360 nM) versus the logarithm of P-SDS concentration.[28]

2.5 Preparation of Cur-Loaded Nano-Micelles (Cur–P-SDS)

Cur-loaded nano-micelles were prepared using a thin-film hydration method. Cur (7 mg), P-SDS complex (93 mg), and Tween 80 (0.05 mg) were dissolved in dichloromethane in a round-bottom flask and stirred for 15 min until a clear solution was obtained. The organic solvent was removed

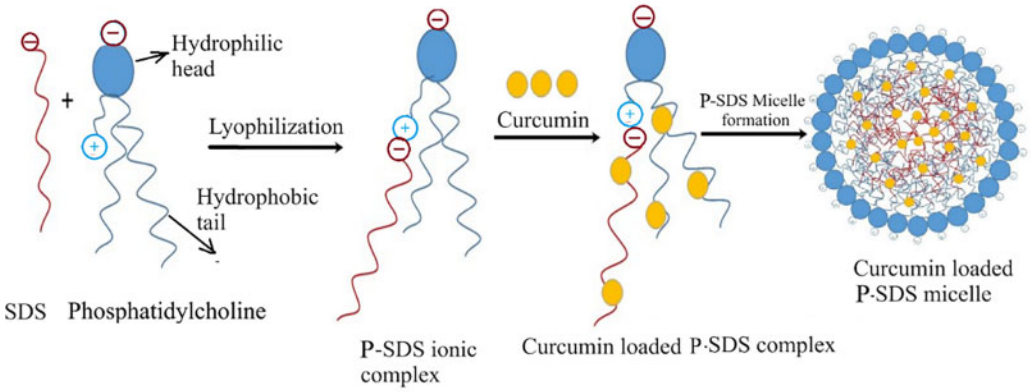


Figure 1. Schematic illustration of the phosphatidylcholine-SDS (P-SDS) ionic complex and Cur-P-SDS formation

using rotary evaporation to form a thin lipid film. The film was further dried under vacuum at 35°C overnight to ensure complete solvent removal. Subsequently, PBS (pH 7.4, 30 mL) was added, and the system was homogenized at 1000 rpm for 15 min to form a uniform nano-dispersion.

2.6 In Vitro Release Assay for Studying Drug-Retention/De-Association

For in vitro release analysis, the freshly prepared Cur–P-SDS dispersion containing 7.6% Cur was distributed equally into 27 Eppendorf tubes (1 mL per tube), corresponding to nine time points with triplicate samples. The samples were incubated at 37°C under orbital shaking (100 rpm) for predetermined time intervals (1, 2, 4, 6, 8, 12, 24, 48, 72, 96, 120 and 144 h). At each time point, one set of tubes was withdrawn and centrifuged at 3000 rpm for 10 min to separate free Cur precipitates from the micellar supernatant.[29] Because Cur is practically insoluble in aqueous media, unencapsulated drug was completely precipitated under these conditions. An aliquot (100 μL) of the supernatant containing P-SDS micelles was collected and diluted in 3.0 mL ethanol for spectrophotometric analysis. Cur concentration was quantified by UV–Vis spectrophotometry at 425 nM. The amount of released drug was calculated by subtracting the encapsulated fraction from the initial loading. Quantification was performed using a calibration curve of Cur in ethanol, constructed over the concentration range of 0.001–0.007 mg/mL. The calibration exhibited good linearity with a correlation coefficient (R^2) of 0.9912. Ethanol was used as the blank reference for all measurements.

The *in vitro* Cur release data were fitted to four kinetic models, including zero-order, first-order, Korsmeyer–Peppas, and Hixson–Crowell models. The goodness of fit for each model was evaluated based on the coefficient of determination (R^2), and the model exhibiting the highest R^2 value was considered to best describe the release kinetics.[30]

2.7 Encapsulation Efficiency and Drug Loading

To evaluate the Cur encapsulation efficiency of the P-SDS micellar system, a series of formulations containing different Cur loadings (7.6%, 13%, 19%, 24.4%, 29.2%, and 33.3% w/w relative to the dry weight of the L-DSD complex) were prepared, each in triplicate (n = 3), following the procedure described above.

Due to the negligible aqueous solubility of Cur, each formulation was subjected to centrifugation at 3000 rpm for 10 min to separate non-encapsulated Cur aggregates from the colloidal dispersion. The resulting supernatant (0.1 mL) was subsequently diluted in 9 mL ethanol to induce complete dissolution ("burst release") of micelle-associated Cur. The amount of encapsulated Cur was quantified using UV–Vis spectrophotometry at 425 nM under ambient conditions. All measurements were performed in triplicate, and the results were reported as mean values. In addition to encapsulation analysis, the average particle size distribution and zeta potential of the P-SDS nano-micelles were determined using dynamic light scattering (DLS) to assess colloidal stability and surface charge behavior. The image of Cur-loaded P-SDS dispersion is provided in supporting information (Figure S1).

Encapsulation efficiency (EE%) and drug loading capacity (DL%) were determined using formulations with varying Cur content.

- $$\text{EE}\,(\%) = (\text{Encapsulated drug/Total drug added}) \times 100 \quad (1)$$

- $$\text{DL}\,(\%) = (\text{Encapsulated drug/Total nanoparticle weight}) \times 100 \quad (2)$$

2.8 Statistical Analysis

All experiments were conducted in triplicate (n = 3), and results are presented as mean ± standard deviation. Statistical significance was evaluated using one-way ANOVA followed by Tukey's post hoc test (GraphPad Prism 5), with $p < 0.05$ considered significant.

3 Results and Discussion

3.1 Formation and Structural Confirmation of P-SDS Ionic Complex

The phosphatidylcholine–SDS (P-SDS) ionic complex was successfully prepared via electrostatic ion-pair interaction between the cationic trimethylammonium group of phosphatidylcholine and the anionic sulfate groups of SDS. This interaction induced a structural rearrangement, resulting in a hybrid amphiphilic architecture with enhanced hydrophobic character compared to native phosphatidylcholine, thereby enabling the design of a wide range of amphiphilic derivatives.[31,32] The prepared P-SDS ionic complex possessed a single anonic head group and three hydrophobic lipid chains. The structural arrangement is expected to enhance drug-loading capacity and steric stability of phosphatidylcholine.

3.1.1 Spectral Analysis

FT-IR spectra provided evidence of ionic interaction. Shifts and intensity variations in phosphate- and sulfate-associated bands indicated strong intermolecular electrostatic interactions. Collectively, spectroscopic results confirmed the formation of a stable ion-paired amphiphilic structure rather than a conventional blended system (Figure S2). Characteristic absorption bands of phosphatidylcholine (C=O 1736 cm^{-1}, P-O-C 1050 cm^{-1}, 1620 cm^{-1} C=C, 1211 cm^{-1} PO_2) and SDS (S=O, 1377 cm^{-1}, C-O-S, 990 cm^{-1}, and 1066 cm^{-1}) are clearly observed. The presence of the characteristic absorption bands of phosphatidylcholine and SDS in the FT-IR spectrum indicates the P-SDS complex formation.[30,33,34]

SDS is insoluble in DCM, while phosphatidylcholine is highly soluble. Thus, the P-SDS ionic complex was isolated by DCM extraction, and the ^{1}H-NMR spectrum in $CDCl_3$ was recorded (Figure 2). ^{1}H NMR analysis confirmed the successful formation of the ionic complex, as characteristic proton signals of both phosphatidylcholine and SDS were simultaneously observed, indicating preservation of molecular integrity.[35] Proton chemical shift of

https://doi.org/10.25135/org.2608.3994
Org. Commun. 2026, 19(4):e26083994

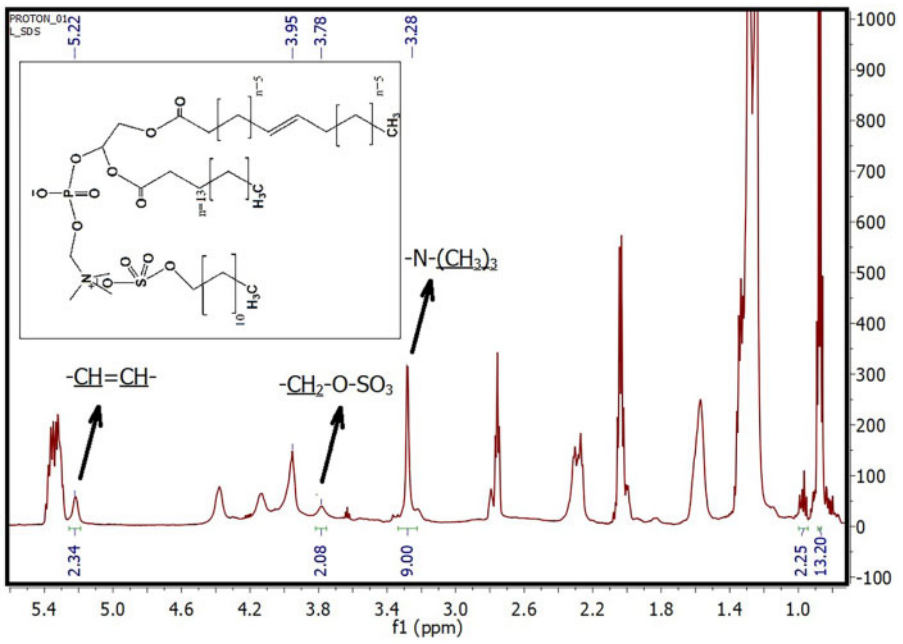


Figure 2. ^{1}H-NMR spectrum of P-SDS ionic complex in $CDCl_3$

phosphatidylcholine in $CDCl_3$ observed in ppm downfield of TMS: 3.28 ppm (-C($\underline{CH_3}$)$_3$), 5.22 ppm (-$\underline{CH}$=$\underline{CH}$-), 0.87 (-$\underline{CH_3}$); proton chemical shift of SDS: 3.78 ppm (-$\underline{CH_2}$-O-SO_3-). 0.87 ppm (-CH_3). The phosphatidylcholine/SDS ratio of the ionic complex was calculated to be nearly 1.0 from the integration values of the -$\underline{CH_2}$-SO_3 (SDS) at 3.78 ppm and the –C(CH_3)$_3$ and –CH=CH- at 3.28 ppm and 5.22 ppm (phosphatidylcholine), respectively. Considering the insolubility of SDS in DCM, the integration ratio further suggested near-stoichiometric association between the two components, supporting stable complex formation rather than simple physical mixing. NMR spectra of pristine phosphatidylcholine and SDS are provided in supporting information (Figure S-3 and S-4).

3.2 Critical Micelle Concentration and Self-Assembly Behavior

Critical Micelle Concentration (CMC) of a surfactant is defined as the minimum concentration value required for the stable micelles formation. Below the CMC, while the amphiphilic molecules spread homogeneously in aqueous medium but above the CMC, self-assembled micelles are formed. CMC can be determined by measuring some physical properties of the aqueous medium, such as surface tension, fluorescence emission, dielectric resistance. The measured properties show rapid changes when the concentration reaches the CMC. Thus, the self-assembly behavior of the P-SDS complex was investigated via fluorescence spectroscopy using pyrene as a fluorophore probe (Figure 3).[28] The obtained CMC value (3.1×10^{-4} M) was significantly lower than that of individual phosphatidylcholine and SDS systems reported in the literature, indicating enhanced thermodynamic stability of the hybrid system. In the literature, the CMC of SDS was reported as 3.5×10^{-2} M,[28,30,33,36] and in

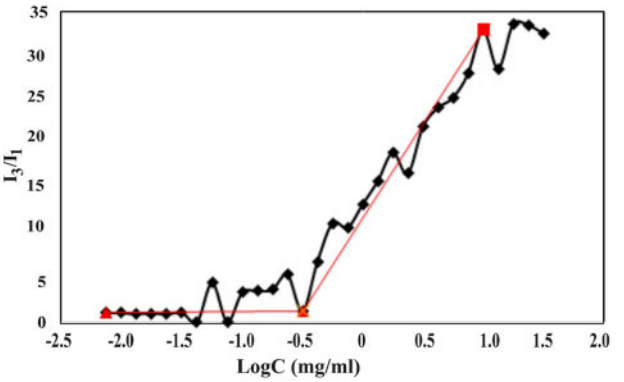


Figure 3. The variation of the ratio of band intensity of the pyrene emission peaks (I_3/I_1) with concentration

our previous study, we determined the CMC of phosphatidylcholine obtained from egg-yolk lecithin as 4.67×10^{-5} M. As reported in the literature, CMC values of lecithin change from 0.2×10^{-3} to 0.15×10^{-1} M depending on the source obtained (i.e., egg-yolk, soybean).[37] This reduction in CMC can be attributed to increased hydrophobic interactions resulting from the coupling of lipid chains from both components, which promotes spontaneous aggregation at lower concentrations. The observed behavior confirms that ionic complexation not only modifies molecular charge distribution but also significantly enhances self-assembly efficiency.[37,38]

3.3 Nano-Micelle Formation and Cur Encapsulation

Another essential property required to be known is the change of particle size with the amount of the drug and how much drug can be loaded inside the core. This amount

Table 1. Encapsulation efficiency data of the formulations and their particle size and zeta potentials

Sample No	Cur* (Wt% of solid)	Cur (mg/mL)	Encapsulated Cur(mg/mL)	Encapsulation Efficiency (%)	Particle size (nM)	Zeta potential
1	7.6	0.2000	0.1296	64.81	239.4	−44.5
2	13.0	0.3571	0.1365	38.22	240.5	−37.4
3	19.0	0.5714	0.2275	39.81	302.4	−40.3
4	24.4	0.7857	0.2275	28.95	621.1	−42.1
5	29.2	1.0000	0.2366	23.66	647.1	−41.4
6	33.3	1.2142	0.2184	17.99	620.7	−42.0

Note: *Cur weight percent was calculated based on the total solids in the formulation. 0.05% of tween-80 was used as an emulsifier in all solid compositions.

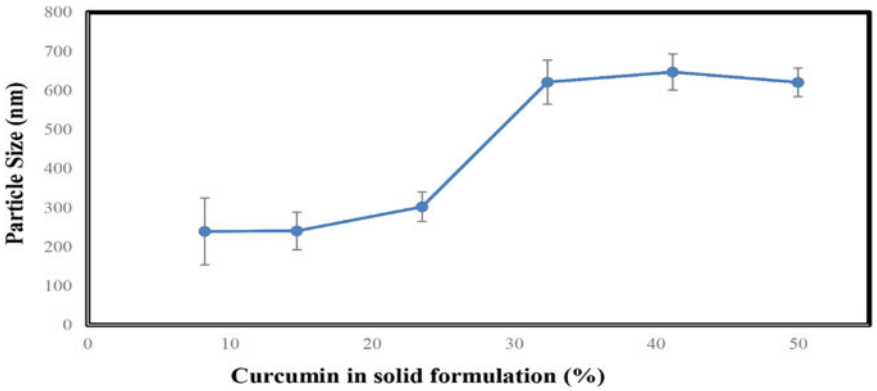


Figure 4. Change of the particle size of Cur-P-SDS with the amount of Cur

is defined as encapsulation efficiency, which is expressed as the percentage of successfully entrapped drugs within the particles. The determined particle size, zeta potential value, and encapsulation efficiency of the Cur-P-SDS micelles with their Cur content are collected in Table 1.

Dynamic light scattering analysis revealed nanoscale particle formation with a mean diameter of 239 nM for the optimized formulation. The system exhibited a strongly negative zeta potential ranging from −37.4 to −44.5 mV, indicating high colloidal stability and electrostatic repulsion between particles, which prevents aggregation. The relatively uniform size distribution (in terms of overall nanoscale morphology) and negative surface charge suggest that Tween-80 plays a stabilizing role by reducing interfacial tension and improving dispersion homogeneity.

Figure 4 shows the change in particle size of the Cur-P-SDS micelles with the amount of Cur loaded. The particle size of the micelles increased with increasing amount of Cur. While no significant change was observed in zeta potential values, the average particle size of the micelles increased up to 41% of Cur content, which was the maximum particle size value, above which a notable change in the particle size of the micelles was not observed. Figure 5 shows the Cur encapsulation efficiency of the P-SDS nano micelles. The encapsulation efficiency decreased with increasing amounts of Cur in formulations. For the formulation initially containing 19 wt% Cur, the encapsulation efficiency was 39.8%, corresponding

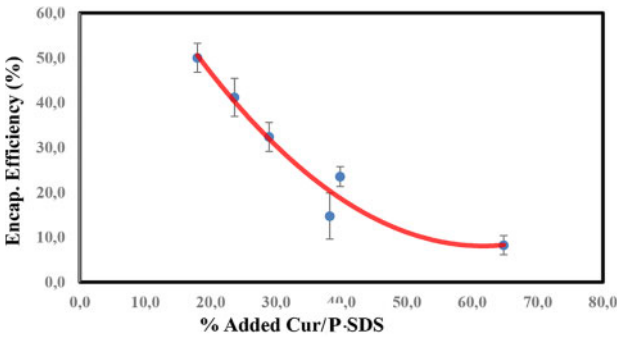


Figure 5. Change of encapsulation efficiency with the percentage of Cur in the formulation

to an effective incorporated Cur content of approximately 7.6 wt% relative to the total formulation solids. These results are consistent with the findings of Chen et al.[7] They reported the values for the lecithin-based self-assembling mixed polymeric micelle dispersions to be less than 200 nM in particle size, greater than 80% of encapsulation efficiency, and greater than 10% of Cur loading capacity. Compared to previously reported lecithin-based or polymeric systems, the P-SDS carrier demonstrated competitive loading performance despite its simpler composition and fully FDA-approved excipient profile.[39]

https://doi.org/10.25135/org.2608.3994
Org. Commun. 2026, 19(4):e26083994

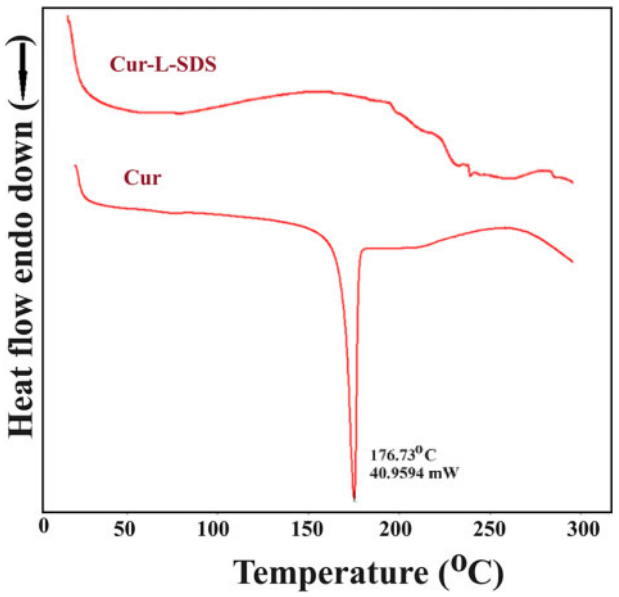


Figure 6. DSC curves of Cur and Cur-loaded P-SDS samples

3.4 Morphology and Physical State of Nano-Micelles

DSC, ESEM, and TEM analyses were performed to elucidate the morphological structure of the Cur-loaded P-SDS ionic complex. DSC curves of Cur and Cur-P-SDS are shown in Figure 6. Cur is a crystalline molecule with a melting point of 176°C. Similarly, the melting point of soybean lecithin was reported as 155°C,[40] and SDS has a melting point of 206°C. Importantly, the complete disappearance of the characteristic melting peak of crystalline Cur (~176°C) in the DSC curve of Cur-P-SDS dry complex indicated the successful molecular dispersion within the lipidic core. This transformation from crystalline to amorphous state of Cur is critical for improving dissolution rate and enhancing bioavailability. Additionally, the absence of thermal transitions corresponding to phosphatidylcholine and SDS further suggests strong molecular interactions and the formation of a unified amorphous stable nano-assembly rather than a physical mixture.[11,33] The TGA curves of the pure components and the P-SDS ionic complex were recorded and are presented in Figures S5–S7. The TGA curve of the P-SDS ionic complex clearly exhibited the characteristic weight-loss steps associated with phosphatidylcholine and SDS (Figure S5–S6), as well as those observed for the individual components (Figure S7).

Figure 7-a and b show the ESEM and TEM images of the 7.6% Cur loaded Cur-P-SDS nano-structured micelles (sample 1 in Table 1) at 50K and 18K magnifications, respectively. ESEM and TEM analyses confirmed the formation of spherical nano-structures with smooth surfaces and heterogeneous morphology. Upon careful examination of the TEM image, the presence of much smaller micelles can also be observed. They have a particle size of under 300 nM. The particle size observed microscopically was consistent with DLS measurements, supporting structural stability in aqueous media. Figure 7-C shows the particle size distribution of the sample (7.6% Cur loaded in Table 1). The polydispersity index (PDI) was determined as 0,525 (Figure 7-c and d). In the TEM images, the presence of smaller non-associated particles that had not fully participated in micellar self-assembly was also observed, which is consistent with the relatively high PDI value of 0.525. These residual nanoscale aggregates likely contributed to the relatively high PDI of the formulation. The negative zeta potential value indicated the negative surface charge of the nano-structured Cur-P-SDS. As reported in the literature, negatively surface-charged nanoparticles undergo endocytosis more efficiently than neutral and positively charged ones.[40] Most solid tumors have a vascular pore cut-off size ranging between 380–780 nM, larger than 300 nM.[41] The nano-structured Cur-P-SDS micelles are promising drug carriers for passive targeting in cancer therapy. Contrary to tumor cells, healthy cell vascularity is impermeable to particulate carriers larger than 4 nM. Therefore, due to this impermeability, the larger particle size of the nano-micelles is a promising advantage in cancer therapy in terms of resulting in less damage to normal cells.[42]

3.5 In Vitro Assay for Studying Drug-Retention/De-Association Assay

This experimental design differs from a conventional dialysis-based in vitro drug release assay. Since there was no separate receptor compartment or semipermeable membrane, the observed profile was not governed by drug transport across a dialysis membrane or by osmotic exchange between donor and receptor compartments. Rather, it primarily reflects the time-dependent retention and release behavior of Cur within the P-SDS micellar dispersion, including processes such as micellar rearrangement, partial destabilization/disassembly, and loss of drug–carrier association under the applied incubation conditions. The percentage release profile of Cur vs time is shown in Figure 8. The Cur–P-SDS nano-micelles exhibited a biphasic release profile characterized by an initial moderate burst release followed by sustained release over 144 hours. Approximately 20% of Cur was released within the first 0.5 hours, attributed to surface-associated drug molecules or molecules that were freely solubilized in the outer aqueous medium. Subsequent release was gradual and controlled, reaching approximately 43% within 10 hours, followed by a plateau-like sustained phase. The final accelerated release phase may be associated with partial destabilization of the micellar structure under prolonged incubation. This release behavior is consistent with lipid-based nanocarriers and is advantageous for maintaining therapeutic drug concentrations over extended periods. The system also demonstrated improved release stability compared to previously reported lecithin- and surfactant-based formulations. In a previous study, a similar release profile of Cur was obtained from an amphiphilic PEG-chitosan graft copolymer-coated poly(D, L-lactic-co-glycolic acid) (PLGA) nanomicelle.[39] A relatively slow release of Cur compared to our results (nearly 20% within 1.0 hours) was observed, and the burst release started after 6.0 hours. In another study,[7] almost 38% of Cur was released within 8.0 hours from the sodium deoxycholate (NaDOC) and lecithin-based self-assembly micelles. The Cur release showed a profound increase after 15.0 hours, and

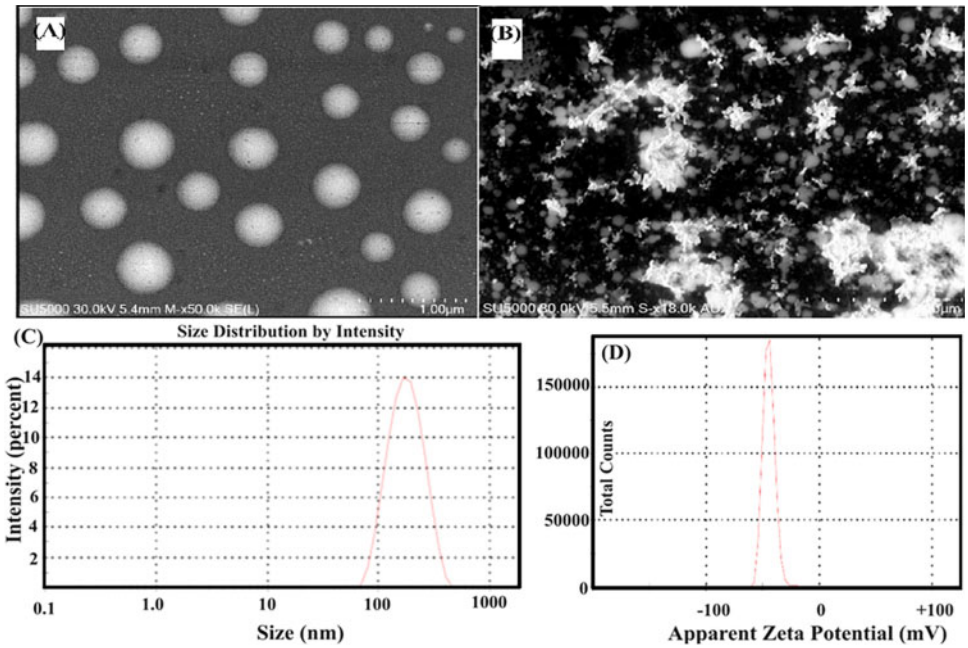


Figure 7. (A) ESEM image, (B) TEM image, (C) Particle size distribution, (D) zeta potential of the sample 7.6% Cur loaded nano-structured P-SDS micelles (sample-1 in Table 1)

nearly 55% of Cur was released after 50 hours. As a result, the P-SDS-based nanostructured self-assembly micelles are more stable than the drug formulations reported in the literature.[43] The sustained release behavior and colloidal stability observed for the Cur–P-SDS nanoassemblies are consistent with recent reports describing lipid-based and amphiphilic micellar systems developed for hydrophobic drug delivery. Recent studies have demonstrated that ionically stabilized amphiphilic nanoassemblies can improve drug retention within the hydrophobic core while simultaneously reducing premature drug leakage into the surrounding aqueous environment.[44,45] Furthermore, phosphatidylcholine-containing nanocarriers have been reported to enhance the amorphous dispersion of hydrophobic therapeutics, thereby improving dissolution characteristics and apparent bioavailability.[46] The relatively low critical micelle concentration observed in the present study further supports the thermodynamic stability of the ion-pair engineered system, which is considered an important parameter for maintaining micellar integrity following dilution under physiological conditions.[38,47]

Several studies have reported that the aqueous solubility of Cur is approximately 0.6 μg/mL.[48–50] On this basis, the concentration of Cur maintained in the aqueous P-SDS micellar dispersion in Sample 1 corresponds to an approximately 216-fold increase relative to the reported intrinsic aqueous solubility of free Cur. We would also like to clarify that the present formulation does not increase the molecular solubility of free Cur in water in the strict thermodynamic sense. Rather, it markedly increases its apparent aqueous solubilization and dispersibility by incorporating Cur into nanoscale P-SDS micellar assemblies. This distinction is important because the principal formulation challenge associated with Cur is precisely its inability to remain dispersed at therapeutically relevant concentrations in aqueous environments.

The mathematical modeling of the Cur release data (Figure 8) showed that the Korsmeyer–Peppas model provided the best fit among the evaluated kinetic models, suggesting that Cur release from the P-SDS nanoassemblies is governed by a complex mechanism rather than by a single zero-order or first-order process. The Korsmeyer–Peppas model is an empirical model commonly applied when drug release involves more than one physicochemical phenomenon, including drug diffusion from the carrier, structural rearrangement or relaxation of the delivery matrix, and gradual destabilization or disassembly of the nanostructure. In the present P-SDS system, the good agreement with this model therefore suggests that Cur release may result from the combined effects of diffusion/desorption of Cur from the micellar domains and time-dependent structural changes in the P-SDS nanoassemblies.

3.6 Colloidal Stability and Biological Relevance

The strong negative zeta potential (−37 to −44 mV) indicates high electrostatic stabilization, which is essential for maintaining dispersion stability in biological fluids. Particle size (~239 nM) places the system within the optimal range for passive tumor targeting via the enhanced permeability and retention (EPR) effect. Additionally, negatively charged nanoparticles may exhibit reduced nonspecific protein adsorption and improved circulation stability compared to neutral systems. The combination of nanoscale size, negative surface charge, and amphiphilic architecture suggests favorable behavior for systemic administration and tumor accumulation.

https://doi.org/10.25135/org.2608.3994
Org. Commun. 2026, 19(4):e26083994

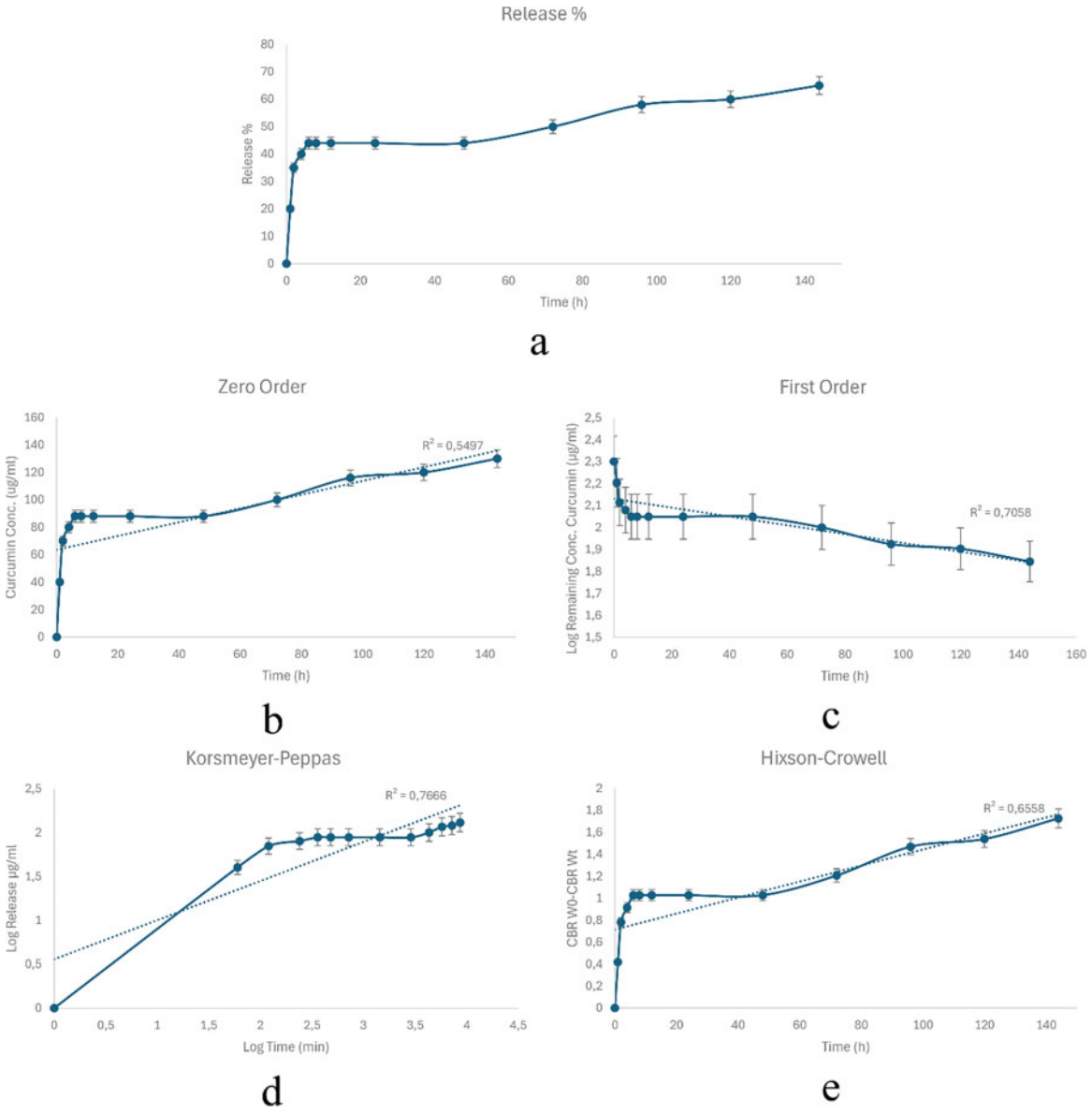


Figure 8. In vitro Cur release profile and kinetic modeling of 7.6% Cur-containing P-SDS nano-micelles (Sample No: 1): (a) cumulative Cur release profile, (b) zero-order, (c) first-order, (d) Korsmeyer–Peppas, and (e) Hixson–Crowell kinetic models. Data are presented as mean ± SD

4 Conclusion

In this study, a novel amphiphilic nanocarrier system was successfully engineered through ionic complexation between phosphatidylcholine and sodium dodecyl sulfate, resulting in the formation of a structurally stable phosphatidylcholine–SDS (P-SDS) ionic complex. This ion-pair strategy enabled a fundamental transformation of phosphatidylcholine from a zwitterionic phospholipid into a highly lipophilic, negatively charged amphiphilic assembly with enhanced self-organization capability. The resulting P-SDS complex exhibited efficient nano-scale self-assembly in the presence of Tween-80, forming stable micellar structures suitable for hydrophobic drug encapsulation. Cur was effectively loaded into the hydrophobic core of the system, achieving amorphous dispersion and complete elimination of crystallinity, which is critical for improving dissolution behavior and bioavailability.

Physicochemical characterization confirmed the formation of a stable nanoformulation with an average particle size of approximately 239 nM and a strongly negative zeta potential (−37 to −44 mV), indicating excellent colloidal stability and suitability for systemic circulation. The low critical micelle concentration further demonstrated the thermodynamic stability of the engineered ionic complex.

In vitro release studies revealed a sustained and controlled release profile over an extended period, supporting the potential of the system for prolonged drug delivery. The encapsulation efficiency and drug loading performance demonstrated that the proposed ionic architecture provides a favorable microenvironment for hydrophobic drug incorporation despite its relatively simple composition. From a

conceptual standpoint, this work introduces a new class of ion-pair lipid–surfactant hybrid nanostructures, where electrostatic complexation is used as a design principle to tune amphiphilicity, self-assembly behavior, and drug-loading capacity. This strategy may be extended to other hydrophobic therapeutic agents beyond Cur, offering a versatile platform for nano-drug delivery applications.

Overall, the developed P-SDS-based nanocarrier represents a scalable, biocompatible, and functionally tunable system with strong potential for targeted anticancer drug delivery via the enhanced permeability and retention (EPR) effect. Furthermore, the simplicity of the fabrication process, together with the use of FDA approved excipients, may provide important translational advantages for future pharmaceutical and biomedical applications.

Funding Statement

This study was supported financially by Marmara University, Scientific Research Projects Committee, with the project number: FEN-C-YLP-200716-0384.

Author Contributions

Mehmet S. Eroglu: Conceptualization, supervision, methodology, formal analysis, reviewing. Aysegul Yargic: Investigation, experimental work, data acquisition. Muge Sennaroglu Bostan: Methodology, investigation, and formal analysis. Fatemeh Bahadori: Conceptualization, methodology, investigation, and writing, review, and editing.

Availability of Data and Materials

The authors declare that the data supporting the findings of this study are available within the paper and its Supplementary Information files. Should any raw data files be needed in another format they are available from the corresponding author upon reasonable request. Source data are provided with this paper.

Artificial Intelligence (AI) Statement

Generative AI tools were used solely for language editing, grammatical improvement, and shortening selected text passages. AI was not used for data generation, data analysis, interpretation of results, or formulation of scientific assumptions or conclusions.

Conflicts of Interest

The authors declare that they do not have any conflict of interest.

Supporting Information

Supporting information accompanies this paper on http://www.acgpubs.org/journals/organic-communications.

ORCID

Aysegul Yargic: 0009-0007-6336-1881
Fatemeh Bahadori: 0000-0003-4224-9309
Muge Sennaroglu Bostan: 0000-0002-2909-689X
Mehmet S. Eroglu: 0000-0003-0742-6162

References

[1] Suri, S. S., Fenniri, H. & Singh, B. (2007). Nanotechnology-based drug delivery systems. *Journal of Occupational Medicine and Toxicology*, *2*(1), 16. DOI: 10.1186/1745-6673-2-16.

[2] Tiwari, G., Tiwari, R., Sriwastawa, B., Bhati, L., Pandey, S., Pandey, P. & Bannerjee, S. K. (2012). Drug delivery systems: An updated review. *International Journal of Pharmaceutical Investigation*, *2*(1), 2. DOI: 10.4103/2230-973x.96920.

[3] Emanuel, N., Kedar, E., Bolotin, E. M., Smorodinsky, N. I. & Barenholz, Y. (1996). Targeted delivery of doxorubicin via sterically stabilized immunoliposomes: Pharmacokinetics and biodistribution in tumor-bearing mice. *Pharmaceutical Research*, *13*(6), 861–868. DOI: 10.1023/a:1016096910822.

[4] Allen, T. M. & Cullis, P. R. (2004). Drug delivery systems: Entering the mainstream. *Science*, *303*(5665), 1818–1822. DOI: 10.1126/science.1095833.

[5] Fang, J., Islam, W. & Maeda, H. (2020). Exploiting the dynamics of the EPR effect and strategies to improve the therapeutic effects of nanomedicines by using EPR effect enhancers. *Advanced Drug Delivery Reviews*, *157*, 142–160. DOI: 10.1016/j.addr.2020.06.005.

[6] Chan, J. M., Zhang, L., Yuet, K. P., Liao, G., Rhee, J.-W., Langer, R. & Farokhzad, O. C. (2009). PLGA–lecithin–PEG core–shell nanoparticles for controlled drug delivery. *Biomaterials*, *30*(8), 1627–1634. DOI: 10.1016/j.biomaterials.2008.12.013.

[7] Chen, L.-C., Chen, Y.-C., Su, C.-Y., Wong, W.-P., Sheu, M.-T. & Ho, H.-O. (2016). Development and characterization of lecithin-based self-assembling mixed polymeric micellar (sa MPMs) drug delivery systems for curcumin. *Scientific Reports*, *6*(1), 37122. DOI: 10.1038/srep37122.

[8] Koifman, N., Schnabel-Lubovsky, M. & Talmon, Y. (2013). Nanostructure formation in the lecithin/isooctane/water system. *The Journal of Physical Chemistry B*, *117*(32), 9558–9567. DOI: 10.1021/jp405490q.

[9] Li, J., Wang, X., Zhang, T., Wang, C., Huang, Z., Luo, X. & Deng, Y. (2015). A review on phospholipids and their main applications in drug delivery systems. *Asian Journal of Pharmaceutical Sciences*, *10*(2), 81–98. DOI: 10.1016/j.ajps.2014.09.004.

[10] Robert, C., Couëdelo, L., Vaysse, C. & Michalski, M.-C. (2020). Vegetable lecithins: A review of their compositional diversity, impact on lipid metabolism and potential in cardiometabolic disease prevention. *Biochimie*, *169*, 121–132. DOI: 10.1016/j.biochi.2019.11.017.

[11] Bahadori, F., Topçu, G., Eroğlu, M. S. & Önyüksel, H. (2014). A new lipid-based nano formulation of vinorelbine. *AAPS PharmSciTech*, *15*(5), 1138–1148. DOI: 10.1208/s12249-014-0146-3.

[12] Vukovic, L., Khatib, F. A., Drake, S. P., Madriaga, A., Brandenburg, K. S., Král, P. & Onyuksel, H. (2011). Structure and dynamics of highly PEG-ylated sterically stabilized micelles in aqueous media. *Journal of the American Chemical Society*, *133*(34), 13481–13488. DOI: 10.1021/ja204043b.

[13] Li, S., Li, Z. & Wang, P. (2016). Experimental study of the stabilization of CO2 foam by sodium dodecyl sulfate and hydrophobic nanoparticles. *Industrial & Engineering Chemistry Research*, *55*(5), 1243–1253. DOI: 10.1021/acs.iecr.5b04443.

[14] Koroleva, M. Y., Karakatenko, E. Y. & Yurtov, E. V. (2020). Synthesis of hydroxyapatite nanoparticles by controlled precipitation in the presence of sodium dodecyl sulfate. *Colloid Journal*, *82*(3), 275–283. DOI: 10.1134/s1061933x20030059.

[15] Fu, W., Qu, F., Yu, G. & You, J. (2017). High selectivity for sodium dodecyl sulphate by polymer nanoparticles and detection of proteins based on the polymer nanoparticles-sodium dodecyl sulphate system. *Sensors and Actuators B: Chemical*, *245*, 774–779. DOI: 10.1016/j.snb.2017.01.175.

[16] Kunchandy, E. & Rao, M. N. A. (1990). Oxygen radical scavenging activity of curcumin. *International Journal of Pharmaceutics*, *58*(3), 237–240. DOI: 10.1016/0378-5173(90)90201-E.

[17] Singh, S. & Aggarwal, B. B. (1995). Activation of transcription factor NF-κB is suppressed by curcumin (diferuloylmethane)(∗). *Journal of Biological Chemistry*, *270*(42), 24995–25000.

[18] Kuo, M.-L., Huang, T.-S. & Lin, J.-K. (1996). Curcumin, an antioxidant and anti-tumor promoter, induces apoptosis in human leukemia cells. *Biochimica et Biophysica Acta (BBA)-Molecular Basis of Disease*, *1317*(2), 95–100. DOI: 10.1016/s0925-4439(96)00032-4.

[19] Somasundaram, S., Edmund, N. A., Moore, D. T., Small, G. W., Shi, Y. Y. & Orlowski, R. Z. (2002). Dietary curcumin inhibits chemotherapy-induced apoptosis in models of human breast cancer. *Cancer Research*, *62*(13), 3868–3875.

[20] Pillai, G. R., Srivastava, A. S., Hassanein, T. I., Chauhan, D. P. & Carrier, E. (2004). Induction of apoptosis in human lung cancer cells by curcumin. *Cancer Letters*, *208*(2), 163–170. DOI: 10.1016/j.canlet.2004.01.008.

[21] Cai, X.-Z., Wang, J., Xiao-Dong, L., Wang, G.-L., Liu, F.-N., Cheng, M.-S. & Li, F. (2009). Curcumin suppresses proliferation and invasion in human gastric cancer cells by down-regulation of PAK1 activity and cyclin D1 expression. *Cancer Biology & Therapy*, *8*(14), 1360–1368. DOI: 10.4161/cbt.8.14.8720.

[22] Shahin, S., Kamboj, A., Anwar, S. & Jain, P. (2012). Nano structure based drug delivery system: An approach to treat cancer. *International Journal of Drug Development and Research*, *4*(2), 393–407.

[23] Nair, R., Kumar, A. C., Priya, V. K., Yadav, C. M. & Raju, P. Y. (2012). Formulation and evaluation of chitosan solid lipid nanoparticles of carbamazepine. *Lipids in Health and Disease*, *11*(1), 72. DOI: 10.1186/1476-511x-11-72.

[24] Goel, A., Kunnumakkara, A. B. & Aggarwal, B. B. (2008). Curcumin as "Curecumin": From kitchen to clinic. *Biochemical Pharmacology*, *75*(4), 787–809. DOI: 10.1016/j.bcp.2007.08.016.

[25] Freitas, C. & Müller, R. H. (1998). Effect of light and temperature on zeta potential and physical stability in solid lipid nanoparticle (SLN™) dispersions. *International Journal of Pharmaceutics*, *168*(2), 221–229. DOI: 10.1016/s0378-5173(98)00092-1.

[26] Sharma, R. A., Ireson, C. R., Verschoyle, R. D., Hill, K. A., Williams, M. L., Leuratti, C., Manson, M. M., Marnett, L. J., Steward, W. P. & Gescher, A. (2001). Effects of dietary curcumin on glutathione S-transferase and malondialdehyde-DNA adducts in rat liver and colon mucosa: Relationship with drug Levels1. *Clinical Cancer Research*, *7*(5), 1452–1458.

[27] U.S. Food and Drug Administration. (2018). [Available from: https://www.fda.gov/food/ingredientspackaginglabeling/foodadditivesingredients/ucm091048.htm.

[28] Kalyanasundaram, K. & Thomas, J. (1977). Environmental effects on vibronic band intensities in pyrene monomer fluorescence and their application in studies of micellar systems. *Journal of the American Chemical Society*, *99*(7), 2039–2044. DOI: 10.1021/ja00449a004.

[29] Bisht, S., Feldmann, G., Soni, S., Ravi, R., Karikar, C., Maitra, A. & Maitra, A. (2007). Polymeric nanoparticle-encapsulated curcumin ("nanocurcumin"): A novel strategy for human cancer therapy. *Journal of Nanobiotechnology*, *5*(1), 3. DOI: 10.1186/1477-3155-5-3.

[30] Vatansever, O., Bahadori, F., Bulut, S. & Eroglu, M. S. (2023). Coating with cationic inulin enhances the drug release profile and in vitro anticancer activity of lecithin-based nano drug delivery systems. *International Journal of Biological Macromolecules*, *237*, 123955. DOI: 10.1016/j.ijbiomac.2023.123955.

[31] Chen, C., Jiang, C. & Tripp, C. P. (2013). Molecular dynamics of the interaction of anionic surfactants with liposomes. *Colloids and Surfaces B: Biointerfaces*, *105*, 173–179. DOI: 10.1016/j.colsurfb.2012.12.045.

[32] Liu, Y., Cao, Z., Wang, J., Zong, W. & Liu, R. (2016). The interaction mechanism between anionic or cationic surfactant with HSA by using spectroscopy, calorimetry and molecular docking methods. *Journal of Molecular Liquids*, *224*, 1008–1015. DOI: 10.1016/j.molliq.2016.10.060.

[33] Mutlu, E. C., Bostan, M. S., Bahadori, F., Kocyigit, A., Oner, E. T. & Eroglu, M. S. (2016). Lecithin-acrylamido-2-methylpropane sulfonate based crosslinked phospholipid nanoparticles as drug carrier. *Journal of Applied Polymer Science*, *133*(42), 44105.

[34] Nzai, J. & Proctor, A. (1999). Soy lecithin phospholipid determination by fourier transform infrared spectroscopy and the acid digest/arseno-molybdate method: A comparative study. *Journal of the American Oil Chemists' Society*, *76*(1), 61–66. DOI: 10.1007/s11746-999-0048-9.

[35] Wałęsa, R., Ptak, T., Siodłak, D., Kupka, T. & Broda, M. A. (2014). Experimental and theoretical NMR studies of interaction between phenylalanine derivative and egg yolk lecithin. *Magnetic Resonance in Chemistry*, *52*(6), 298–305. DOI: 10.1002/mrc.4064.

[36] Bisht, S., Feldmann, G., Soni, S., Ravi, R., Karikar, C., Maitra, A. & Maitra, A. (2007). Polymeric nanoparticle-encapsulated curcumin ("nanocurcumin"): A novel strategy for human cancer therapy. *Journal of Nanobiotechnology*, *5*, 1–18.

[37] Walde, P., Blöchliger, E. & Morigaki, K. (1999). Circular dichroic properties of phosphatidylcholine micelles. *Langmuir*, *15*(7), 2346–2350. DOI: 10.1021/la9810814.

[38] Chakraborty, T., Chakraborty, I. & Ghosh, S. (2011). The methods of determination of critical micellar concentrations of the amphiphilic systems in aqueous medium. *Arabian Journal of Chemistry*, *4*(3), 265–270. DOI: 10.1016/j.arabjc.2010.06.045.

[39] El-Sherbiny, I. M. & Smyth, H. D. (2012). Controlled release pulmonary administration of curcumin using swellable biocompatible microparticles. *Molecular Pharmaceutics*, *9*(2), 269–280. DOI: 10.1021/mp200351y.

[40] Eladawy, N. O., Morsi, N. M. & Shamma, R. N. (2021). Diacerein-loaded hyaluosomes as a dual-function platform for osteoarthritis management via intra-articular injection: In vitro characterization and in vivo assessment in a rat model. *Pharmaceutics*, *13*(6), 765. DOI: 10.3390/pharmaceutics13060765.

[41] Oh, N. & Park, J.-H. (2014). Endocytosis and exocytosis of nanoparticles in mammalian cells. *International Journal of Nanomedicine*, *9*(suppl1), 51–63. DOI: 10.2147/ijn.s26592.

[42] Anitha, A., Deepagan, V. G., Rani, V. V. D., Menon, D., Nair, S. V. & Jayakumar, R. (2011). Preparation, characterization, in vitro drug release and biological studies of curcumin loaded dextran sulphate–chitosan nanoparticles. *Carbohydrate Polymers*, *84*(3), 1158–1164. DOI: 10.1016/j.carbpol.2011.01.005.

[43] Bahadori, F., Topçu, G., Eroğlu, M. S. & Önyüksel, H. (2014). A new lipid-based nano formulation of vinorelbine. *AAPS PharmSciTech*, *15*, 1138–1148. DOI: 10.1208/s12249-014-0146-3.

[44] Jacob, S., Kather, F. S., Morsy, M. A., Boddu, S. H., Attimarad, M., Shah, J., Shinu, B. & Nair, A. B. (2024). Advances in nanocarrier systems for overcoming formulation challenges of curcumin: Current insights. *Nanomaterials*, *14*(8), 672. DOI: 10.3390/nano14080672.

[45] Zhou, Q., Zhang, L., Yang, T. & Wu, H. (2018). Stimuli-responsive polymeric micelles for drug delivery and cancer therapy. *International Journal of Nanomedicine*, *13*, 2921–2942. DOI: 10.2147/ijn.s158696.

[46] Grüne, L. & Bunjes, H. (2024). Solubility of poorly soluble drugs in phosphatidylcholine-based drug delivery systems: Comparison of the loading capacity in the bulk formulation and its dispersed state. *Pharmaceuticals*, *17*(3), 400. DOI: 10.3390/ph17030400.

[47] Chatterjee, A., Moulik, S., Sanyal, S., Mishra, B. & Puri, P. (2001). Thermodynamics of micelle formation of ionic surfactants: A critical assessment for sodium dodecyl sulfate, cetyl pyridinium chloride and dioctyl sulfosuccinate (Na salt) by microcalorimetric, conductometric, and tensiometric measurements. *The Journal of Physical Chemistry B*, *105*(51), 12823–12831. DOI: 10.1021/jp0123029.

[48] Cysewski, P. (2019). Natural deep eutectic solvents as agents for improving solubility, stability and delivery of curcumin. *arXiv preprint arXiv: 190602105*.

[49] Górnicka, J., Mika, M., Wróblewska, O., Siudem, P. & Paradowska, K. (2023). Methods to improve the solubility of curcumin from turmeric. *Life*, *13*(1), 207. DOI: 10.3390/life13010207.

[50] Kurien, B. T., Singh, A., Matsumoto, H. & Scofield, R. H. (2007). Improving the solubility and pharmacological efficacy of curcumin by heat treatment. *Assay and Drug Development Technologies*, *5*(4), 567–576. DOI: 10.1089/adt.2007.064.